Article ID: 1000-7032(2023)09-1693-12

A Ratiometric Fluorescent Polystyrene Microsphere Hybrid Probe for Highly Selective Detection of Anthrax Markers

HU Runze[1], XU Chen[1], FANG Zhou[1], LI Ying[1*], MIN Hua[2*]

(1. *School of Materials & Chemistry, University of Shanghai for Science and Technology, Shanghai* 200093, *China*;
2. *Technology Transfer Center, Institute of Science and Technology Development, University of Shanghai for Science and Technology, Shanghai* 200093, *China*)

* *Corresponding Authors, E-mail: liying@usst. edu. cn*; 13801784422@163. *com*

Abstract: $Eu(DBM)_3Phen$ was firstly encapsulated into carboxylated polystyrene microspheres by the encapsulation method, and then the lanthanide luminescence center Tb^{3+} was introduced by coordination to obtain the fluorescent polystyrene microsphere hybrid probe Tb-PS@$Eu(DBM)_3Phen$ with dual emission centers. The results indicated that Tb-PS@$Eu(DBM)_3Phen$ has excellent stability, dispersibility and fluorescence properties. In addition, by further investigating the fluorescence sensing properties of the probe molecule on 2, 6-pyridinedicarboxylic acid (DPA), it was found that Tb-PS@$Eu(DBM)_3Phen$ could produce a significant enhancement with the present of DPA, which might be due to the coordination of terbium ions on the surface of DPA and polystyrene microspheres, which in turn affected the energy transfer process between the ligand-rare earths, resulting in Tb-PS@$Eu(DBM)_3Phen$'s fluorescence enhancement. Meanwhile, Tb-PS@$Eu(DBM)_3Phen$ has strong selectivity and anti-interference ability for DPA, which is expected to be used as a potential fluorescent probe for the recognition of DPA.

Key words: lanthanide complexes; fluorescent microspheres; DPA; ratiometric fluorescent sensing
CLC number: TB333 **Document code**: A **DOI**: 10. 37188/CJL. 20230049

一种比率型荧光聚苯乙烯微球杂化探针用于炭疽病毒标志物的高选择性检测

胡润泽[1], 徐 陈[1], 方 舟[1], 李 颖[1*], 闵 华[2*]

(1. 上海理工大学 材料与化学学院, 上海 200093; 2. 上海理工大学科技发展研究院 技术转移中心, 上海 200093)

摘要: 采用包埋法将通过二苯甲酰甲烷(DBM)和1-10无水邻菲啰啉(Phen)制得的稀土配合物$Eu(DBM)_3Phen$包埋进羧基化聚苯乙烯微球中,再通过配位作用引入镧系发光中心Tb^{3+},获得具有双发射中心的荧光聚苯乙烯微球杂化探针Tb-PS@$Eu(DBM)_3Phen$。利用SEM、TEM、FT-IR、XPS、UV-Vis、PL等表征方法对探针分子的结构和性能进行分析。研究结果表明,Tb-PS@$Eu(DBM)_3Phen$具有优异的稳定性、分散性和荧光性能。此外,通过进一步研究探针分子对2,6-吡啶二甲酸(DPA)的荧光传感性能,发现DPA能够对Tb-PS@$Eu(DBM)_3Phen$的荧光产生明显的增强效果,这可能是由于DPA和聚苯乙烯微球表面的铽离子配位,进而使配体-稀土之间的能量传递过程受到影响,从而造成Tb-PS@$Eu(DBM)_3Phen$的荧光增强。同时,Tb-PS@$Eu(DBM)_3Phen$对DPA具有较强的选择性和抗干扰能力,有望用作检测识别DPA的荧光探针。

收稿日期: 2023-03-01; **修订日期**: 2023-03-13
基金项目: 国家自然科学基金(21101107,51173107); 同济大学污染控制与资源化国家重点实验室基金项目(PCRRF19017)
Supported by National Natural Science Foundation of China(21101107,51173107); State Key Laboratory of Pollution Control and Resource Reuse Foundation(PCRRF19017)

关 键 词：稀土配合物；荧光微球；DPA；比率荧光传感

1 Introduction

Despite that various means of preventing anthrax, it still represents a considerable public health hazard to the world community[1-3]. Anthrax is known to be an infectious disease caused by the bacterium Bacillus anthracis, which can cause fatal infection if more than 10^4 spores are inhaled in a 36 h period. Bacillus anthracis belongs to the genus bacillus aerobicus which is a rod-shaped, gram-positive bacterium that can not only be ubiquitous in soil but also persist for decades, surviving for long periods of time even under extreme adverse conditions such as high temperatures, strong UV radiation, and strong acidic or alkaline conditions[4-5]. In addition, once the surrounding environment meets its growth requirements, anthrax bacilli are activated and spread rapidly. Humans can contract anthrax in a number of ways, including inhalation of anthrax spores, contact with anthrax-contaminated materials, and consumption of inadequately heated meat from sick animals resulting in intestinal anthrax. Therefore, anthracis is considered a potentially extremely lethal biological warfare agent and has received widespread international attention[6]. As a major component of bacterial spores, 2,6-pyridinedicarboxylic acid(DPA) accounts for 5%−15% of the dry mass of spores and is not found in other natural or synthetic materials, so it can be used as a typical anthrax biomarker[7-8]. Therefore, exploring an efficient and accurate DPA assay is of great importance.

Several methods have been developed for the detection of DPA, including surface-enhanced Raman spectroscopy(SERS)[9], polymerase chain reaction(PCR)[10], superparamagnetic cross-flow immunoassay(LFA) [11], gas chromatography/mass spectrometry (GC/MS)[12], and electrochemical detection[13]. However, traditional detection methods, such as HPLC and GC/MS, require specialized operators, complex sample preparation and expensive instruments, and LFA and PCR require more demanding procedures and expensive chemicals, which may be a barrier to practical application and are not suitable for commercial use. In contrast, fluorescence detection has become a more economically competitive option that attributed to its low cost, ease of operation, high selectivity and sensitivity, fast response time and real-time monitoring[14-16].

Due to the unique spectral properties of rare earth ions, such as long fluorescence lifetime, large Stokes shift and narrow emission band, fluorescence sensors based on rare earth ions have been developed rapidly[17-20]. In particular, two rare earth elements, Eu^{3+} and Tb^{3+}, located in the visible region. In recent years, nanomaterials functionalized based on these two rare earth ions have been used for the detection of DPA[21-23]. However, as a single emission sensor to detect DPA is susceptible to interference from background light, temperature, instrumentation, and other external conditions that affect the results of detection[24]. Fortunately, ratiometric fluorescent probes can be color adjusted and self-calibrated by measuring fluctuations in the ratio of fluorescence intensity at two wavelengths, thus eliminating environmental or instrumental interference and increasing the accuracy of detection results and are considered ideal tools for building sensing platforms[25-28]. Fluorescent microspheres[29-33] with their stable morphological structure and stable and efficient luminescence efficiency[34-35], have been used in labeling, intelligence analysis, detection immobilized enzymes, immunological medicine, and high-throughput drug screening[36-40]. In particular, fluorescent microspheres using polystyrene microspheres as a substrate have many advantages of polystyrene microspheres themselves. For instances, large specific surface area, good stability, strong surface reactivity, and easy surface functionalization. In addition, the surface of microspheres can relate to different bioactive macromolecules, which in turn can be widely used in biomarkers, fluorescent probes, bioimaging, fluorescent sensors and immunoassays[41]. Therefore,

in this thesis, a ratiometric fluorescent probe Tb-PS@Eu(DBM)$_3$Phen was synthesized using Eu^{3+} as the reference fluorescence, introducing europium complexes into the interior of polystyrene microspheres in the form of encapsulation, and then ligating with terbium ions through carboxyl groups on the surface of polystyrene microspheres. Compared with measurements performed at a single wavelength, it has strong anti-interference properties and avoids the influence of external factors such as the instrument, the dose of the detector and temperature on the results, enabling the sensitive detection of the bacillus anthracis biomarker DPA.

2　Experiment

2.1　Preparation of Tb-PS@Eu(DBM)$_3$Phen

2.1.1　Experimental Reagents

$NaHCO_3$, MMA, $K_2S_2O_8$, anhydrous ethanol, benzoic acid, isophthalic acid, homo-phthalic acid, glutamine, glycine, 3,4-pyridinedicarboxylic acid, 2,4-pyridinedicarboxylic acid, 3,5-pyridinedicarboxylic acid MAA, $LnCl_3 \cdot 6H_2O$, L-Aspartic acid.

2.1.2　Preparation Process

(1) Purification of styrene

To reduce the polymerization loss of styrene monomer, polymerization inhibitors are often added to styrene. Therefore, it is necessary to purify styrene with alkaline alumina before use. We take an appropriate amount of alkaline alumina in the chromatographic column, add 100 mL of styrene in the column to remove the polymerization inhibitor. The purified styrene is put in a dry and clean reagent bottle, and stored in the refrigerator at 2−8 ℃.

(2) Preparation of rare earth complex Eu(DBM)$_3$-Phen

6 mmol of dibenzoylmethane, 2 mmol of 1-10 anhydrous phloroglucinol and 6 mmol of sodium hydroxide were mixed into 40 mL of anhydrous ethanol and placed in an oil bath to dissolve with stirring. When it was warmed up to 50 ℃, 20 mL of ethanol solution dissolved with 2 mmol $EuCl_3 \cdot 6H_2O$ was added slowly dropwise and the mixture was refluxed at 50 ℃ for another 2 h. The mixture was left to reaction for 3 h and then filtered by brinell funnel extraction and washed several times with ethanol/water. The resulting solid powder was dried at 60 ℃ for 12 h.

(3) Synthesis of carboxylated fluorescent microspheres PS@Eu(DBM)$_3$Phen

Carboxylated fluorescent polystyrene microspheres were prepared using soap-free emulsion polymerization method and embedding method. First, water (32 mL), $NaHCO_3$ (0.24 mg), methacrylate (0.85 mL containing Eu(DBM)$_3$Phen(40 mg)) and styrene(2 mL) were placed in a 100 mL three-neck flask. After purging with nitrogen for 30 min, the temperature was gradually increased to 80 ℃ and 2 mL(0.01 g) of aqueous potassium persulfate solution was added. Then, after 30 min reaction, 0.2 mL of methacrylic acid and 2 mL(0.01 g) of aqueous potassium persulfate were added. Finally, the reaction was continued for 10 h and cooled to room temperature.

(4) Preparation of fluorescent microspheres Tb-PS@Eu(DBM)$_3$Phen

At the end of the above experiment, $TbCl_3 \cdot 6H_2O$(0.1 g) was added to continue the reaction for 1 h. Finally, the reaction was cooled to room temperature and washed alternately with alcohol and water and redispersed in ethanol(Fig. 1).

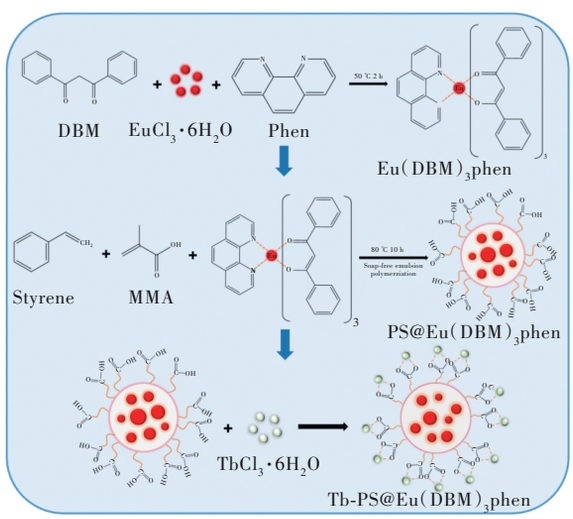

Fig.1　Experimental flow chart of Tb-PS@Eu(DBM)$_3$Phen

(5) Fluorescence sensing detection of DPA by Tb-PS@Eu(DBM)$_3$Phen

30 mg of Tb-PS@Eu(DBM)$_3$Phen powder was dissolved in 10 mL of anhydrous ethanol and sonicated

for 5 min to disperse uniformly to form a clear suspension. Under the same experimental conditions, the fluorescence of Tb-PS@Eu(DBM)$_3$Phen was also measured at the excitation wavelength of 280 nm.

In the anti-interference experiments, the Tb-PS@Eu(DBM)$_3$Phen solutions were prepared in the same way as the above experiments, except that 100 μL of other substances with similar structures of different species (concentrations of 20 μmol/L) were added, respectively, including benzoic acid (BEN), isophthalic acid (IPA), homo-phthalic tricarboxylic acid (BTC), L-aspartic acid (L-ASP), glutamic acid (GLC), glycine (GLY), 3,4-pyridinedicarboxylic acid (3,4-PCA), 2,4-pyridinedicarboxylic acid (IA), and 3,5-pyridinedicarboxylic acid (3,5-PCA).

2.2 Performance and Characterization of Tb-PS@Eu(DBM)$_3$Phen

The Fourier Transform Infrared Spectroscopy (FT-IR) was measured by the American Nexus 912 AO446 spectrometer, and the solid samples were prepared by KBr tablet technology. The fluorescence intensity was measured by the Japanese RF-5301PC spectrophotometer, and the xenon lamp was used as the excitation light source. X-ray photoelectric spectrometry (XPS) was measured by the American Thermo Scientific K-Alpha spectrometer. The ultraviolet-visible spectrum (UV-Vis) was measured by the American Lambda 750 spectrometer, and the sample was deionized water as the solvent. Scanning electron microscope (SEM) measurements were conducted on a Sigma 300 at an accelerating voltage of 20 kV. Fluorescence lifetime was measured by Edinburgh FLS1000.

3 Results and Discussion

3.1 Structural Characterization of Tb-PS@Eu(DBM)$_3$Phen

The formation of Tb-PS@Eu(DBM)$_3$Phen can be verified by the FT-IR spectrum in Fig. 2. As can be seen that an absorption band at 1 740 cm^{-1} is observed in the Tb-PS@Eu(DBM)$_3$Phen spectrum, which can be attributed to the C═O absorption peak. Also, the methylene absorption peak of polystyrene microspheres appears at 2 924 cm^{-1}, indicating the successful polymerization of methacrylic acid with polystyrene. In addition, 1 606 cm^{-1} could be contributed to the skeletal vibrational absorption peak of the benzene ring. The characteristic absorption of C—O located at 1 453 cm^{-1} and 1 492 cm^{-1}, respectively, indicating that the complex Eu(DBM)$_3$-Phen has been successfully introduced into the carboxylated polystyrene microsphere table. The Tb—O stretching vibrational peak appears in the fingerprint region (450–500 cm^{-1}) indicating the successful grafting of Tb onto the surface of polystyrene microspheres[42-43].

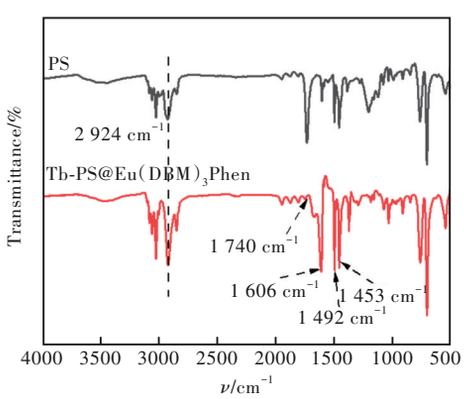

Fig.2 FT-IR spectra of Tb-PS@Eu(DBM)$_3$Phen and PS

Further analysis of XPS results of Tb-PS@Eu(DBM)$_3$Phen as shown in Fig. 3(a). The characteristic peaks of C 1s, N 1s, O 1s, Tb 3d, and Eu 3d appear at 283.08, 316.08, 531.4, 1 257.7, 1 134.94 eV. This indicates that Tb-PS@Eu(DBM)$_3$Phen is composed of five elements: carbon, nitrogen, oxygen, terbium and europium, with elemental contents of 91.52%, 1.16%, 6.87%, 0.19% and 0.26%, which also further confirmed the successful binding of Tb^{3+} and Eu^{3+} to the PS. In addition, the high-resolution XPS spectra indicated that the Tb-PS@Eu(DBM)$_3$Phen in the carbon element was presented as C═C (284.7 eV) and C—O (286.2 eV) and O═C═O (288.4 eV) (Fig. 3(b))[44-45], and the nitrogen element was presented as N—Eu (400.4 eV) (Fig. 3(c))[46], while oxygen elements are presented as C═O (531.3 eV), C—O/C—OH (532.2 eV) and *M*—O (*M*=Tb, Eu) groups (530.5 eV) (Fig. 3(d))[47].

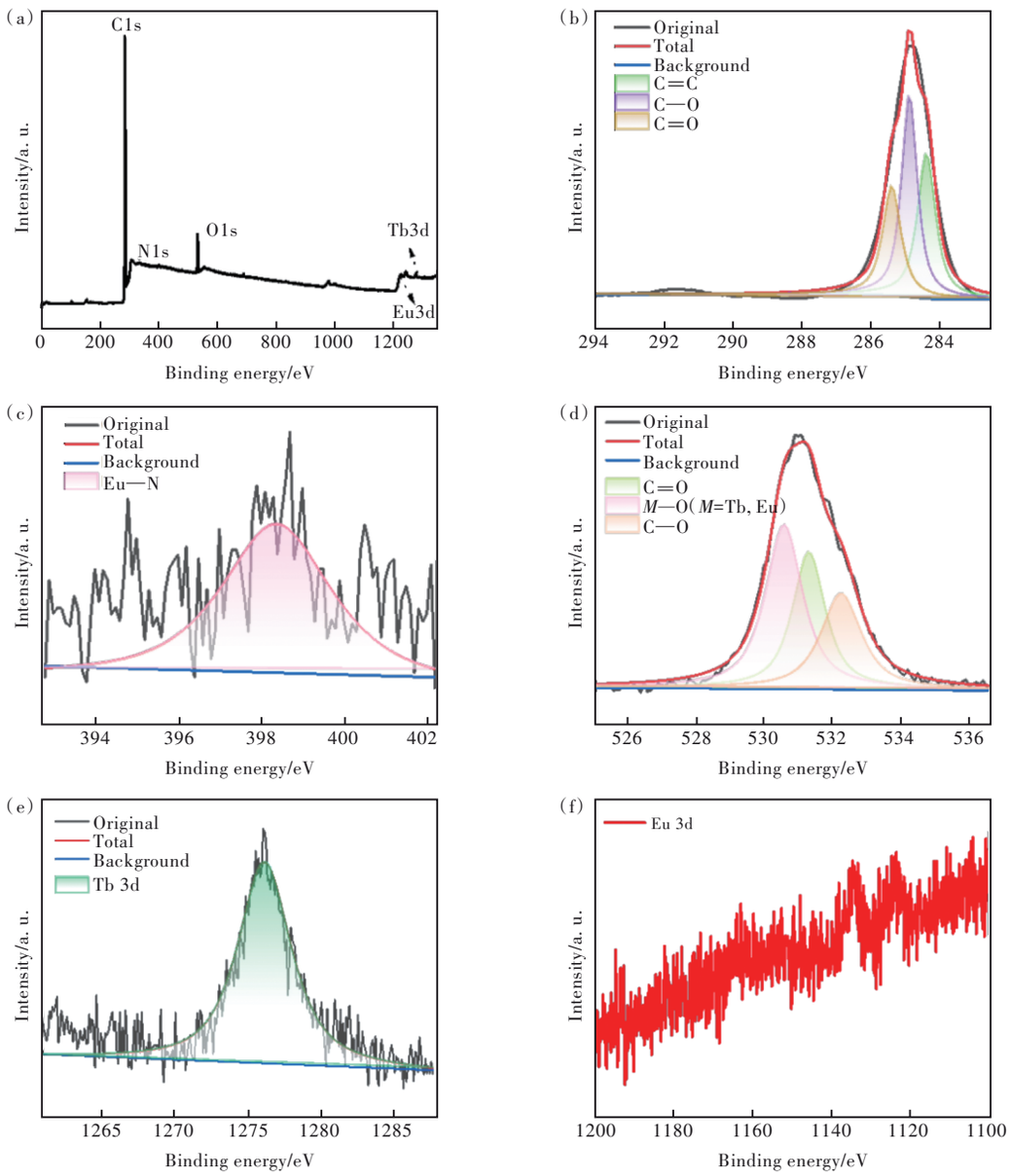

Fig. 3　(a)XPS full spectrum of Tb-PS@Eu(DBM)$_3$Phen. (b)C 1s fine spectra. (c)N 1s fine spectra. (d)O 1s fine spectra. (e) Tb 3d fine spectra. (f)Eu 3d fine spectrum.

Fine spectra of Tb 3d and Eu 3d were also observed (Fig. 3(e)-(f)), and XPS analysis results were consistent with FT-IR spectra.

3.2　Morphological Characterization of Tb-PS@Eu(DBM)$_3$Phen

As illustrated in Fig. 4, the SEM image of the scale 2 μm Tb-PS@Eu(DBM)$_3$Phen, it can be observed that the prepared polystyrene fluorescent microspheres have a spherical morphology and uniform microsphere size with good dispersion. The SEM image of PS@Eu(DBM)$_3$Phen is revealed in the Fig. 4(a). According to the typical preparation method, the polystyrene microspheres carrying carboxyl groups on the surface were synthesized by the polymerization method of soap-free emulsion. And the fluorescent polystyrene microspheres PS@Eu(DBM)$_3$-Phen were prepared by introducing the complex Eu-(DBM)$_3$Phen in the encapsulation form during the polymerization process. It can be observed that the prepared microspheres have a uniform size of 300 nm and are well dispersed. Finally, the ratiometric fluorescent polystyrene microspheres Tb-PS@Eu-(DBM)$_3$Phen with dual luminescence centers were obtained by using the carboxyl groups on the surface

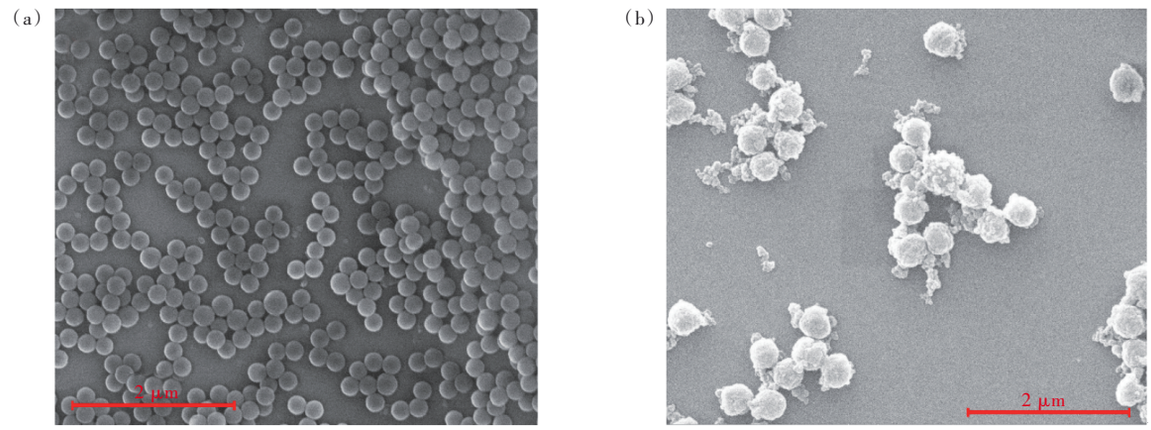

Fig.4 SEM images of PS@Eu(DBM)$_3$Phen(a) and Tb-PS@Eu(DBM)$_3$Phen(b)

ligated with terbium ions, and the particle size was increased to 350 nm (Fig. 4(b)).

3.3 Fluorescence Properties Analysis of Tb-PS@Eu(DBM)$_3$Phen

The fluorescence excitation and emission spectra of PS@Eu(DBM)$_3$Phen were given in Fig. 5(a). When excited at 294 nm, four narrow characteristic emission spectra exhibit the 4f→4f transitions of Eu^{3+} ($^5D_0 \rightarrow {}^7F_J$, J =1-4), which located at 596, 611, 651, 703 nm, respectively. The most intense emission peak at 611 nm is ascribed to $^5D_0 \rightarrow {}^7F_2$ transition, and it induced the red emissions. PS@Eu(DBM)$_3$-Phen can be observed to exhibit a bright red color under a 365 nm UV lamp. Fig. 5(b) displays the fluorescence excitation and emission spectra of Tb-PS@Eu(DBM)$_3$Phen, and it can be observed that the optimal excitation wavelength becomes 280 nm, grafted onto the surface of polystyrene microspheres.

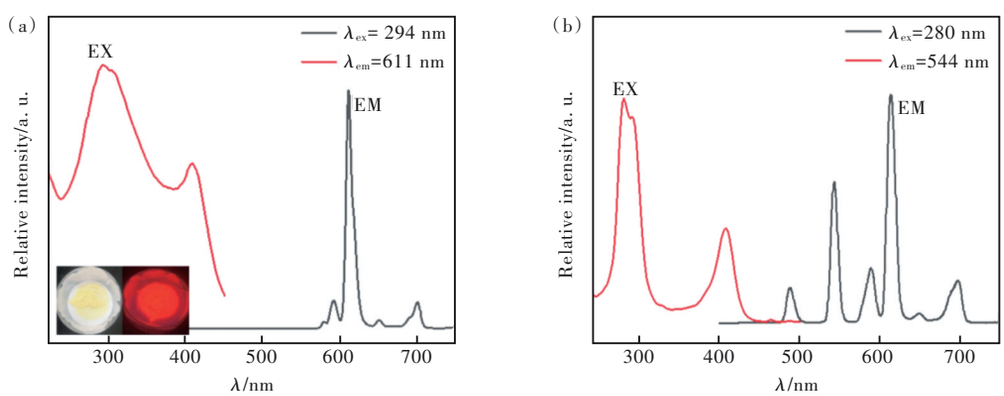

Fig.5 Fluorescence emission patterns of PS@Eu(DBM)$_3$Phen(a) and Tb-PS@Eu(DBM)$_3$Phen(b)

3.4 Sensing Detection of DPA by Tb-PS@Eu-(DBM)$_3$Phen

(1) Detection feasibility analysis

The feasibility of detecting DPA was investigated by comparing the fluorescence emission profiles of Tb-PS@Eu(DBM)$_3$Phen and Tb-PS@Eu(DBM)$_3$-Phen + DPA. As exhibited in Fig. 6, the fluorescence emission intensity at 615 nm was less changed after the addition of DPA molecules to Tb-PS@Eu(DBM)$_3$Phen, and the fluorescence emission intensity at 544 nm was effectively enhanced. Meanwhile, the change of the probe from red to green could be clearly observed by the naked eye under the UV lamp irradiation, and these results confirmed the good feasibility of the probe in the detection of DPA.

(2) Optimization of the detection conditions

The optimal detection conditions were obtained by optimizing the two parameters (equilibration time and temperature) that affect the detection efficiency, as shown in Fig. 7. The concentration of the detector DPA was uniformly controlled as 20 μmol/L. Firstly, the effect of equilibration time corresponding to the fluorescence intensity effect was investigated, as

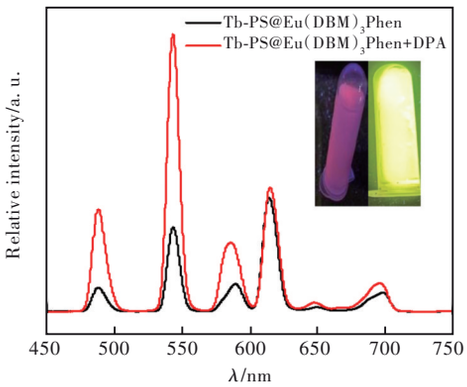

Fig.6　Fluorescence emission pattern of Tb-PS@Eu(DBM)$_3$-Phen before and after the addition of PA

shown in the figure, the fluorescence intensity of the probe Tb-PS@Eu(DBM)$_3$Phen varied almost 0 within 0–20 min, indicating that the prepared probe has good time stability, as shown in Fig. 7(a). Next, the temperature stability of the probe was investigated, as shown by Fig. 7(b), the fluorescence intensity of the probe Tb-PS@Eu(DBM)$_3$Phen decreased with the gradual increase of temperature within 10–45 ℃. Therefore, for the accuracy of the measurement we chose the transient detection at room temperature conditions.

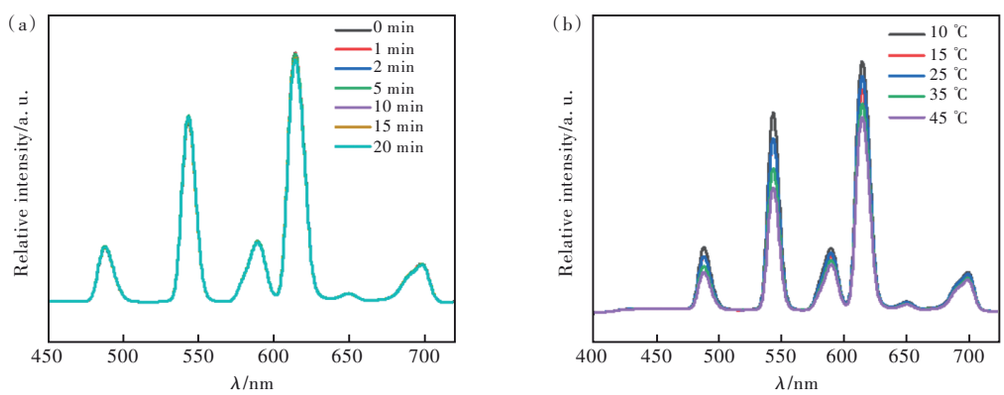

Fig.7　Effect of temperature and time on the fluorescence intensity of Tb-PS@Eu(DBM)$_3$Phen

(3) Titration of DPA concentration and calculation of detection limit

Sensitivity is an important factor affecting the effect of fluorescent probes, therefore, in this thesis, the fluorescence emission spectra of Tb-PS@Eu-(DBM)$_3$Phen were measured after adding different concentrations of DPA solution.

The fluorescence emission spectra of Tb-PS@Eu-(DBM)$_3$Phen after the addition of different concentrations of DPA solution were analyzed, and the results were descripted in Fig. 8(a). Obviously, when the concentration of DPA solution was in the range of 1–100 μmol/L, the fluorescence intensity at 544 nm was gradually enhanced with the increase of DPA concentration, and the fluorescence intensity at 615 nm was almost unchanged. In addition, we found that when the DPA concentration was in the range of 20–70 μmol/L, there was a good linear relationship between I_{615}/I_{544} and DPA concentration which can be calculated by the Stern-Volmer equation as

$$\frac{I_{615}}{I_{544}} = 1 + K_{SV}C, \tag{1}$$

where C is the concentration of DPA, K_{SV} is the Stern-Volmer constant, and I_{615} and I_{544} are the fluorescence intensity at 615 nm and 544 nm before and after the addition of DPA, respectively. As shown in Fig. 8(b), the regression equation was obtained as I_{615}/I_{544}=0.00472C+0.72549 (R^2=0.997 01) by linear fitting. The limit of detection (D) of the probe was calculated from the 3σ equation to be as low as 1.32 μmol/L:

$$D = \frac{3\sigma}{S}, \tag{2}$$

σ is the standard deviation obtained from 20 consecutive scans of the blank solution. S is the slope of the linear equation. The good linear correlation and low detection limits imply that Tb-PS@Eu(DBM)$_3$-Phen sensor has higher sensitivity and excellent detection capability for DPA.

(4) Specificity and selectivity of detection

Specificity and selectivity are also another important indicator of the effectiveness of fluorescent

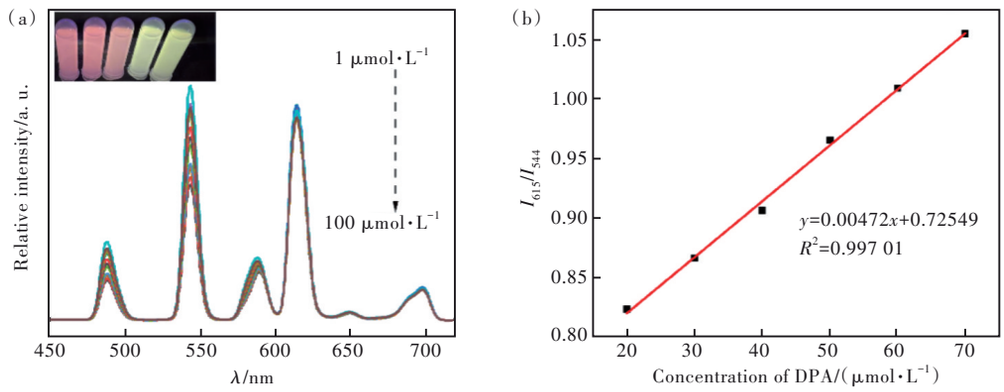

Fig. 8 The emission spectra of Tb-PS@Eu(DBM)$_3$Phen at different concentrations of DPA(a) and the linear relationship between peak fluorescence intensity ratio and DPA concentration(b)

probes. The selectivity of the Tb-PS@Eu(DBM)$_3$-Phen probe for DPA was explored by selecting several other analogues including BEN, IPA, BTC, L-ASP, GLC, GLY, 3,4-PCA, IA, and 3,5-PCA. As illustrated in Fig. 9(a), several other substances exhibited different degrees of fluorescence enhancement responses. However, the fluorescence enhancement of DPA was obviously higher than that of several other substances(Fig. 9(b)). This may be attributed to the terbium ion on the surface of the probe Tb-PS@Eu(DBM)$_3$Phen has the strongest binding ability to DPA (F indicates the fluorescence intensity after the addition of different substances, and F_0 represents the fluorescence intensity of the Tb-PS@Eu(DBM)$_3$Phen at 544 nm). Therefore, these results suggest that Tb-PS@Eu(DBM)$_3$-Phen can be considered as a potential fluorescent sensor with good specificity and selectivity.

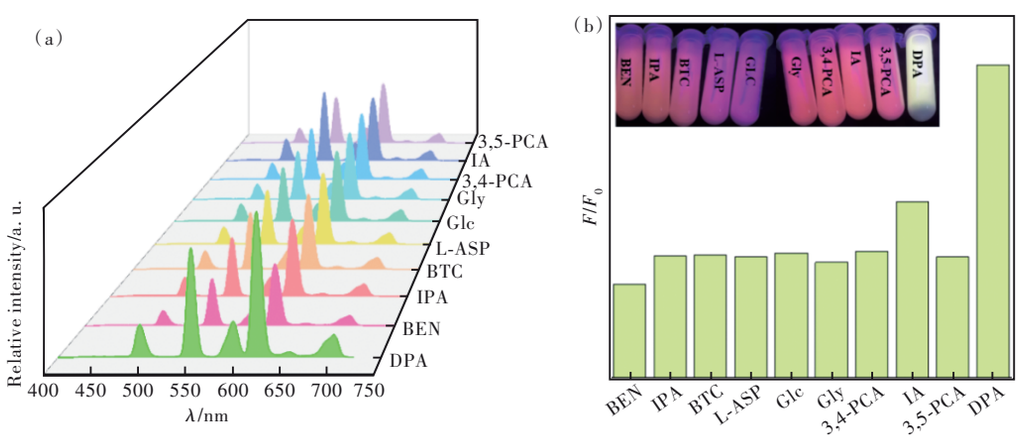

Fig. 9 The emission spectra of Tb-PS@Eu(DBM)$_3$Phen after adding different substances(a) and the histogram of fluorescence change after adding different substances(b)

(5) Detection mechanism

The energy transfer between the ligand and the central ion is the main reason for the fluorescence enhancement mechanism. The possible mechanism of fluorescence enhancement for Tb-PS@Eu(DBM)$_3$-Phen by DPA may be attributed to the antenna effect. Since the coordination between PS@Eu(DBM)$_3$-Phen and Tb^{3+} in Tb-PS@Eu(DBM)$_3$Phen is unsaturated, water molecules occupy the empty coordination center of Tb^{3+}, leading to the quenching emission of Tb^{3+}. The organic ligand DPA with β-diketone structure can chelate to the central Tb^{3+} ions by coordinating bond as a co-ligand(Fig. 10(d)). In addition, the fluorescence lifetime of Tb-PS@Eu(DBM)$_3$-Phen has been tested to further illustrated that the introduction of DPA can improve the fluorescence properties of the samples(Fig. 10(b)-(c)).

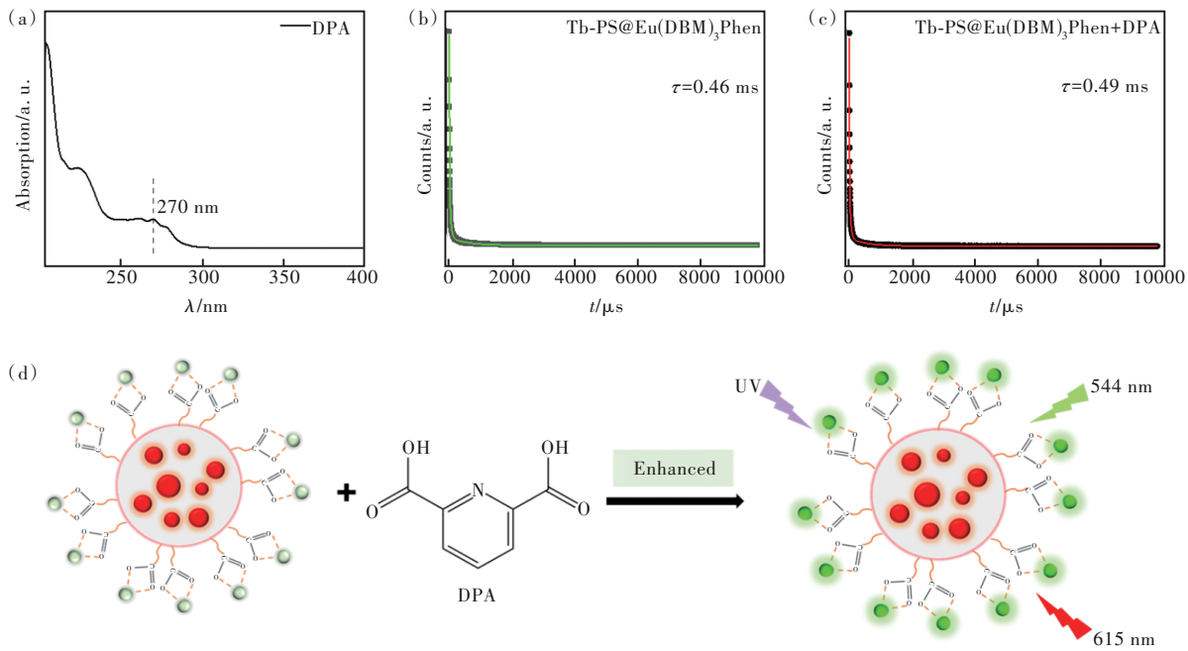

Fig. 10　(a)UV-Vis spectrum of DPA. Fluorescence lifetime of Tb-PS@Eu(DBM)$_3$Phen(b) and Tb-PS@Eu(DBM)$_3$Phen + DPA (c). (d)Mechanism of DPA detection by Tb-PS@Eu(DBM)$_3$Phen.

4　Conclusion

In summary, we constructed a lanthanide-based ratiometric fluorescent probe Tb-PS@Eu(DBM)$_3$-Phen. By further investigating the fluorescence sensing performance of the probe molecule on DPA, it was found that DPA can produce a significant enhancement effect on the fluorescence of Tb-PS@Eu-(DBM)$_3$Phen. Meanwhile, Tb-PS@Eu(DBM)$_3$Phen has strong selectivity and anti-interference ability for DPA with good linearity in 20−70 μmol/L and low detection limit 1.32 μmol/L, which is potential to develop into a fluorescent sensor for visual detection of DPA .

Response Letter is available for this paper at:http://cjl. lightpublishing. cn/thesisDetails#10. 37188/CJL. 20230049.

References:

[1] KUMITA K, KITAZAWA Y, TOKUDA R, *et al.* First report of anthracnose on tillandsia caused by Colletotrichum sp. in Japan [J]. *J. Gen. Plant Pathol.*, 2021, 87(4): 254−258.

[2] CUSTÓDIO F A, BROMMONSCHENKEL T C, SILVA A D A, *et al.* Colletotrichum pereskiae sp. nov. causing anthracnose on pereskia aculeata in Brazil [J]. *Mycol. Prog.*, 2021, 20(12): 1583-1593.

[3] MAHADEVAKUMAR S, CHANDANA C, JANARDHANA G R. First report of Colletotrichum truncatum associated with anthracnose disease on tuberose (Polianthes tuberosa) in India [J]. *Crop Prot.*, 2019, 118: 1-5.

[4] BARANDONGO Z R, DOLFI A C, BRUCE S A, *et al.* The persistence of time: the lifespan of Bacillus anthracis spores in environmental reservoirs [J]. *Res. Microbiol.*, 2023, doi: 10. 1016/J. RESMIC. 2023. 104029.

[5] BRAUN P, KNÜPFER M, ANTWERPEN M, *et al.* A rare glimpse into the past of the anthrax pathogen Bacillus anthracis [J]. *Microorganisms.*, 2020, 8(2): 298-1-7.

[6] COSTANTINO V, BAHL P, DOOLAN C, *et al.* Modeling on the effects of deliberate release of aerosolized inhalational Bacillus anthracis (anthrax) on an Australian Population [J]. *Health Secur.*, 2023, 21(1): 61-69.

[7] SHIPMAN M A, RAMHIT K J, BLIGHT B A. Sensing a Bacillis anthracis biomarker with well-known OLED emitter EuTta$_3$Phen [J]. *J Mater. Chem.* B, 2016, 4(18): 3043-3045.

[8] VERMA M, KAUR N, SINGH N. Naphthalimide-based DNA-coupled hybrid assembly for sensing dipicolinic acid: a biomarker for Bacillus anthracis spores [J]. *Langmuir*, 2018, 34(22): 6591-6600.

[9] ZHANG X Y, YOUNG M A, LYANDRES O, *et al*. Rapid detection of an anthrax biomarker by surface-enhanced Raman spectroscopy [J]. *J. Am. Chem. Soc*, 2005, 127(12): 4484-4489.

[10] LARKIN I N, GARIMELLA V, YAMANKURT G, *et al*. Dual-readout sandwich immunoassay for device-free and highly sensitive anthrax biomarker detection [J]. *Anal. Chem.*, 2020, 92(11): 7845-7851.

[11] WANG D B, TIAN B, ZHANG Z P, *et al*. Rapid detection of Bacillus anthracis spores using a super-paramagnetic lateral-flow immunological detectionsystem [J]. *Biosens. Bioelectron.*, 2013, 42: 661-667.

[12] LINS R C, BOYER A E, KUKLENYIK Z, *et al*. Zeptomole per milliliter detection and quantification of edema factor in plasma by LC-MS/MS yields insights into toxemia and the progression of inhalation anthrax [J]. *Anal. Bioanal. Chem.*, 2019, 411(12): 2493-2509.

[13] FARROW B, HONG S A, ROMERO E C, *et al*. Correction to a chemically synthesized capture agent enables the selective, sensitive, and robust electrochemical detection of anthrax protective antigen [J]. *ACS Nano*, 2018, 12(5): 5066-5066.

[14] WANG Y Q, FANG, Z, MIN, H, *et al*. Sensitive determination of ofloxacin by molecularly imprinted polymers containing ionic liquid functionalized carbon quantum dots and europium ion [J]. *ACS Appl. Nano Mater.*, 2022, 5(6): 8467-8474.

[15] LI Y, LING H X, GAO Y, *et al*. Lanthanide β-diketonate complex functionalized poly(ionic liquid)s/SiO_2 microsphere as a fluorescent probe for the determination of bovine hemoglobin [J]. *ACS Appl. Polym. Mater.*, 2022, 4(4): 2941-2950.

[16] GAN Z Y, HU X T, HUANG X W, *et al*. A dual-emission fluorescence sensor for ultrasensitive sensing mercury in milk based on carbon quantum dots modified with europium (III) complexes [J]. *Sens. Actuators* B *Chem.*, 2021, 328: 128997-1-9.

[17] GU D X, YANG W T, LIN D Y, *et al*. Water-stable lanthanide-based metal-organic gel for the detection of organic amines and white-light emission [J]. *J. Mater. Chem.* C, 2020, 8(39): 13648-13654.

[18] SAHOO J, JAISWAR S, CHATTERJEE P B, *et al*. Mechanistic insight of sensing hydrogen phosphate in aqueous medium by using lanthanide(III)-based luminescent probes [J]. *Nanomaterials*, 2021, 11(1): 53-1-13.

[19] LI Z, LU S, LI X J, *et al*. Lanthanide upconversion nanoplatforms for advanced bacteria-targeted detection and therapy [J]. *Adv. Opt. Mater.*, 2023, 11(11): 2202386.

[20] LUO L, XIE Y, HOU S L, *et al*. Recyclable luminescent sensor for detecting creatinine based on a lanthanide-organic framework [J]. *Inorg. Chem.*, 2022, 61(26): 9990-9996.

[21] HALAWA M I, LI B S, XU G B. Novel synthesis of thiolated gold nanoclusters induced by lanthanides for ultrasensitive and luminescent detection of the potential anthrax spores' biomarker [J]. *ACS Appl. Mater. Interfaces*, 2020, 12(29): 32888-32897.

[22] DONMEZ M, YILMAZ M D, KILBAS B. Fluorescent detection of dipicolinic acid as a biomarker of bacterial spores using lanthanide-chelated gold nanoparticles [J]. *J. Hazard. Mater.*, 2017, 324: 593-598.

[23] LUAN K, MENG R Q, SHAN C F, *et al*. Terbium functionalized micelle nanoprobe for ratiometric fluorescence detection of anthrax spore biomarker [J]. *Anal. Chem.*, 2018, 90(5): 3600-3607.

[24] CAI K Y, ZENG M L, LIU F F, *et al*. BSA-AuNPs@Tb-AMP metal-organic frameworks for ratiometric fluorescence detection of DPA and Hg^{2+} [J]. *Luminescence*, 2017, 32(7): 1277-1282.

[25] LI Z J, LIU G, FAN C B, *et al*. Ratiometric fluorescence for sensitive detection of phosphate species based on mixed lanthanide metal organic framework [J]. *Anal. Bioanal. Chem.*, 2021, 413(12): 3281-3290.

[26] LIU X W, LI X, XU S L, *et al*. Efficient ratiometric fluorescence probe based on dual-emission luminescent lanthanide coordination polymer for amyloid β-peptide detection [J]. *Sens. Actuators* B *Chem.*, 2022, 352: 131052.

[27] SUN X C, CONG Z Z, WU S Y, *et al*. Stable lanthanide metal-organic frameworks as ratiometric fluorescent probes for the efficient detection of riboflavin [J]. *J. Mater. Chem.* C, 2022, 10(41): 15516-15523.

[28] SUN Y Y, DRAMOU P, SONG Z R, *et al.* Lanthanide metal doped organic gel as ratiometric fluorescence probe for selective monitoring of ciprofloxacin [J]. *Microchem. J.*, 2022, 179: 107476-1-8.

[29] CHENG Y H, CAI Z Y, XU Z H, *et al.* Smart sensing device for formaldehyde that based on uniform lanthanide CPs microsphere [J]. *J. Mol. Struct.*, 2023, 1281: 135004.

[30] XU K, LIN C, QIN M F, *et al.* Amplifying photoluminescence of lanthanide-doped nanoparticles by iridium phosphonate complex [J]. *ACS Mater. Lett.*, 2023, 5(3): 854-861.

[31] LI X, TANG J, WANG G J, *et al.* Facile synthesis and luminescence properties of lanthanide ions doped gadolinium phosphate hierarchical hollow spheres [J]. *Solid State Sci.*, 2020, 107: 106354-1-8.

[32] ZHAO S, TIAN R R, SHAO B Q, *et al.* One-pot synthesis of Ln^{3+}-doped porous BiF_3@PAA nanospheres for temperature sensing and pH-responsive drug delivery guided by CT imaging [J]. *Nanoscale*, 2020, 12(2): 695-702.

[33] ZHAO X, SHAO B Q, TANG J, *et al.* Green synthesis and luminescence properties of lanthanide ions doped yttrium oxyfluoride microdiscs [J]. *Appl. Surf. Sci.*, 2019, 484: 285-292.

[34] 刘权, 李子坚, 赵旭东, 等. 稀土掺杂中红外硫系光纤及其传感应用研究进展 [J]. 硅酸盐学报, 2022, 50(4): 1100-1108.
LIU Q, LI Z J, ZHAO X D, *et al.* Progress on rare-earth ions doped midinfrared chalcogenide optical fibers and their sensing application [J]. *J. Chin. Ceramic Soc.*, 2022, 50(4): 1100-1108. (in Chinese)

[35] XIE M J, CHEN Z L, ZHAO F G, *et al.* Selection and application of ssDNA Aptamers for fluorescence biosensing detection of malachite green [J]. *Foods*, 2022, 11(6): 801-1-15.

[36] 刘丽, 胡润泽, 徐陈, 等. 镧系 Eu^{3+}配合物修饰的分子印迹聚合物荧光探针制备及其对血红蛋白的传感检测 [J]. 发光学报, 2022, 43(6): 944-951.
LIU L, HU R Z, XU C, *et al.* Preparation of molecularly imprinted polymer fluorescence probe modified by lanthanide Eu^{3+} complex and hemoglobin sensing detection [J]. *Chin. J. Lumin.*, 2022, 43(6): 944-951. (in Chinese)

[37] SANKOVA N, SHALAEV P, SEMEYKINA V, *et al.* Spectrally encoded microspheres for immunofluorescence analysis [J]. *J. Appl. Polym. Sci.*, 2020, 138(8): 49890-1-21.

[38] YIN J X, DENG J Q, WANG L, *et al.* Detection of circulating tumor cells by fluorescence microspheres-mediated amplification [J]. *Anal. Chem.*, 2020, 92(10): 6968-6976.

[39] SONG L P, ZHANG, L, XU K, *et al.* Fluorescent microsphere probe for rapid qualitative and quantitative detection of trypsin activity [J]. *Nanoscale Adv.*, 2019, 1(1): 162-167.

[40] 蒙铭周, 张瑞, 法信蒙, 等. Ce^{3+}掺杂对 $NaYF_4$:Yb^{3+},Tm^{3+}纳米粒子上转换发光性能的影响及其荧光温度特性应用 [J]. 发光学报, 2021, 42(11): 1763-1773.
MENG M Z, ZHANG R, FA X M, *et al.* Effect of Ce^{3+} doping on upconversion luminescence of $NaYF_4$: Yb^{3+}, Tm^{3+} nanoparticles and application of fluorescence temperature characteristics [J]. *Chin. J. Lumin.*, 2021, 42(11): 1763-1773. (in Chinese)

[41] MONDAL T K, MONDAL S, GHORAI U K, *et al.* White light emitting lanthanide based carbon quantum dots as toxic Cr (VI) and pH sensor [J]. *J. Colloid Interface Sci.*, 2019, 553: 177-185.

[42] SONG T, ZHANG Q, LU C L, *et al.* Structural design and preparation of high-performance QD-encoded polymer beads for suspension arrays [J]. *J. Mater. Chem.*, 2011, 21(7): 2169-2177.

[43] 邵可满, 傅桂瑜, 陈素艳, 等. 稀土配合物分子印迹荧光探针的制备及检测孔雀石绿的残留 [J]. 光谱学与光谱分析, 2022, 42(3): 808-813.
SHAO K M, FU G Y, CHEN S Y, *et al.* Preparation of molecularly imprinted fluorescent probe for rare earth complex and determination of malachite green residue [J]. *Spectrosc. Spect. Anal.*, 2022, 42(3): 808-813. (in Chinese)

[44] DANG V D, GANGANBOINA A B, DOONG R A. Bipyridine- and copper-functionalized N-doped carbon dots for fluorescence turn off-on detection of ciprofloxacin [J]. *ACS Appl. Mater. Interfaces*, 2020, 12(29): 32247-32258.

[45] XU F Z, TANG H Y, YU J H, *et al.* A Cu^{2+}-assisted fluorescence switch biosensor for detecting of coenzyme a employing nitrogen-doped carbon dots [J]. *Talanta*, 2021, 224: 121838-1-7.

[46] YANG J, JIN X L, CHENG Z, *et al.* Facile and green synthesis of bifunctional carbon dots for detection of Cu^{2+} and ClO^-

in aqueous solution [J]. *ACS Sustainable Chem. Eng.*, 2021, 9(39): 13206-13214.

[47] 彭晓, 阳维维, 凌东雄, 等. 红色荧光粉$Sr_3LiSbO_6:Eu^{3+}$制备及其发光性质[J]. 发光学报, 2021, 42(4): 455-461.
PENG X, YANG W W, LING D X, *et al*. Preparation and luminescence properties of red $Sr_3LiSbO_6:Eu^{3+}$ phosphor [J]. *Chin. J. Lumin.*, 2021, 42(4): 455-461. (in Chinese)

胡润泽(1996-),男,江苏宿迁人,硕士研究生,2020年于南通大学获得学士学位,主要从事稀土荧光杂化材料的研究。
E-mail: hrz13806293487@163.com

闵华(1975-),男,上海人,硕士,高级技术经纪人,2015年于上海理工大学获得硕士学位,主要从事电气自动化及控制、技术转移转化。
E-mail: 13801784422@163.com

李颖(1981-),女,内蒙古乌兰浩特人,博士,副教授,硕士生导师,2009年于同济大学获得博士学位,主要从事稀土/高分子荧光杂化材料及其生物化学传感应用的研究。
E-mail: liying@usst.edu.cn